Proceedings of the 2026 16th International Pipeline Conference
IPC2026
September 21-25, 2026, Calgary, Alberta, Canada

IPC2026-110495

TIME-DOMAIN SPECTRAL ELEMENT SIMULATION OF LAMB WAVE TIME REVERSAL METHOD FOR DETECTING A BREATHING CRACK IN A PLATE

Zexing Yu[1], Fei Du[1], Chao Xu[1]

[1]School of Astronautics of Northwestern Polytechnical University, Xi'an, China

ABSTRACT

Lamb wave is considered as an appropriate approach to detect the cracks in structures. This paper combines an efficient time-domain spectral finite element with time reversal method to develop an efficient breathing crack detection method. In this regard, Gauss-Lobatto-Legendre quadrature rules and penalty function method are carried out to construct an effective and accurate approach. Comparing the computation scales and results of this method and traditional finite element method, the validity and superiority of the proposed model is stressed. The reconstructed signals of two scenarios, intact and impaired structures, are captured. It is concluded that, this approach is capable of detecting breathing cracks. In addition, the influences of the relative depth of the notch and incident region are studied. This research may provide the guidance for experiment configuration and the further study.

Keywords: Lamb waves; time reversal focusing; time-domain spectral element finite method; breaking crack; nonlinear waves

1. INTRODUCTION

Breathing cracks are great threats to structures, since they grow quickly and are hard to detect. Hence, many crack detection strategies have been developed in structural health monitoring. Lamb waves have been regarded as an effective way to detect the defects in structures because it can propagate over long distance and carry damage information without much attenuation [1]. However, the phenomenon, such as scattering, emission, dispersion and reflection, brings difficulties for recording and analyzing the signal in wave propagation [2]. Time reversal method can eliminate these drawbacks and establish a kind of so-called baseline-free damage detection method, which is superior in signal-to-noise ratio [3]. The process of time reversal can be simply expressed as that, a signal can be reconstructed at the excitation point if a response is reversed in time domain and reemitted to the excitation point. The principle and mathematical derivation of time reversibility can be found in many literatures [4, 5].

Time reversal method has been widely used in the field of structural health monitoring as a mature technology. H. W. Park et al combined time reversal method and wavelet-based signal processing to detect the defects in composite plates [6]. In their study, based on the Mindlin plate theory, a time reversal operator is introduced to enhance the time reversal method and their work is validated by the experimental results. B. Poddar et al developed baseline-free damage identification method by using the Lamb wave and time reversal method [7]. The influences of many parameters, such as frequency, band width, the size of sensors and tuning, are studied by experimental tools. The results show that some damages like notch, block mass and surface erosion in the wave path break the time reversibility. Hence, the distortion of waveform can be an indicator for defects. Wang et al developed an artificial time-reversal array to overcome the main drawback of traditional time reversal method, which cannot precisely reconstruct the profiles of input signals in the case of flexural waves [8]. The results demonstrate that their method has a better robustness and may reduce the sensor density without the decreasing of measured accuracy.

Detection of cracks using Lamb waves and time reversal method relates to a complex study. It requires numerical method to predict the nonlinear wave propagation and decide preferred indicators[9].The time-domain spectral finite element method (SFEM) has been used to simulate the wave propagation in different scenarios, which was proposed by Patera in fluid dynamics firstly [10]. This method can be viewed as a special type of FE method and bears some similarity with the *p*-version FE method [11]. The main idea of this method is the implementation of a special high-order interpolation function. In each spectral finite element, the inner interpolation nodes are collocated non-uniformly at the Gauss-Lobatto-Legendre (GLL) points, which coordinates are relative to the first derivative of *nth* Legendre polynomial. In this regard, the significant drawback of high-order FE method in solving wave propagation called Runge's phenomenon can be effectively suppressed [12]. However, to the best of the authors' knowledge, there are few

SAMPLE

Copyright © 2025 ASME

studies related to the crack detection using SFEM and time reversal method.

This paper takes advantages of the SFEM and time reversal method to develop an efficient breathing crack detection approach. Firstly, a contact spectral element is derived to model the separate cracks. The proposed method is validated by traditional finite element method (FE method) and the efficiency is addressed by comparing the mesh scale. The results demonstrate that this method can detect cracks and has potential to identify the depth and location of cracks.

2. THE TIME-DOMAIN SPECTRAL FINITE ELEMENT METHOD FOR BREATHING CRACKS

As shown in Fig. 1, there is a 4th order time-domain spectral finite element. The interpolation nodes are nonlinear configured at the element, different from the traditional finite element condition. This feature eliminates the influence the Runge's phenomenon, which indicates a problem of oscillation near the edges of an interval that occurs when using polynomial interpolation with polynomials of high degree over a set of nodes spaced in a uniform grid. Hence, the high-order Lagrange polynomial function is available for SFEM without critical errors and fast convergence of dynamic simulation is achieved. For the proposed element, the coordinates of interpolation nodes are determined by GLL nodes, which are the roots of the following formulation:

$$(1-\xi\xi^2)\underset{mn}{PP'}(\xi\xi), \text{ and } (1-\eta\eta^2)\underset{mn}{PP'}(\eta\eta) \quad (1)$$

where $\underset{mn}{PP'}(\xi\xi)$, and $\underset{mn}{PP'}(\eta\eta)$ represent the first derivative of the mth order Legendre polynomial in two main direction, respectively.

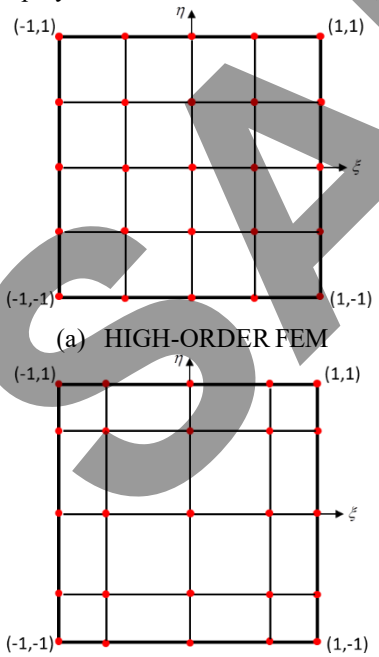

(a) HIGH-ORDER FEM

(b) HIGH-ORDER SEM

FIGURE 1: THE COMPARISON OF TRADITIONAL FEM AND PROPOSED SEM

The governing equation obtained by Hamilton principle is:

$$\mathbf{MM}\ddot{q} + \mathbf{CC}\dot{q} + \mathbf{KK}q = \mathbf{FF}(t) \quad (2)$$

where $\mathbf{MM}$, $\mathbf{CC}$, $\mathbf{KK}$ and $\mathbf{FF}(t)$ denote the mass matrix, damp matrix, stiffness matrix and external force vector, respectively and $\boldsymbol{qq}$ is the displacement vector. The definitions of matrices are expressed in many literatures and will not be described here.

A plate with length L, thickness h and width b is illustrated in Fig. 2. At the middle of the plate, there is a single edge notch, which is V-shaped and depth is dd_{cc}. The surfaces of crack touch each other under the influence of external load and then separate when force is unloaded. The behavior is defined as the 'breathing' of cracks. In this regard, the matrices of open cracks are determined by the linear element and the Jocabian matrix is carried out to distinguish the notch element. When the crack closes, the separable hard contact model is used to simulate the contact nonlinearity.

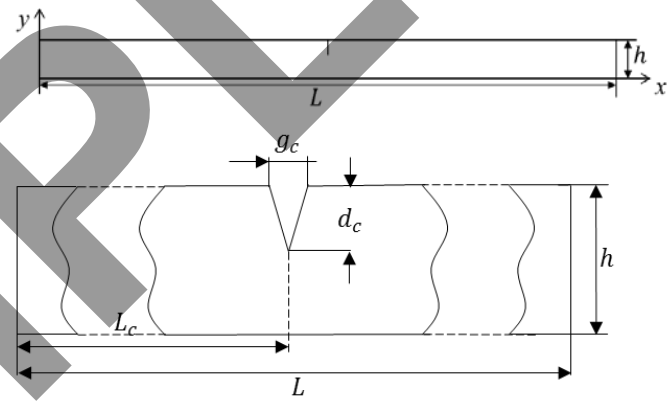

FIGURE 2: DIAGRAM OF PLANE WITH A NOTCH.

In the case of crack model, the energy relationship of two contact surfaces can be expressed as:

$$\Pi = U - W + G \quad (3)$$

where Π, U and W denote the total energy, strain energy and external work, respectively. G is constraining item for the nonlinear contact. Based on the variation principle, the total energy gets extremum when:

$$\delta\Pi = \delta U - \delta W + \delta G = 0 \quad (4)$$

the variations of stress energy and external work parts are:

$$\delta U = \int_{VV} (\delta\delta\delta\delta)^{TT}\, \sigma dV \quad (5)$$

$$\delta W = \int_{VV} (\delta\delta\delta\delta)^{TT} PPddPP + \int_{\Gamma} (\delta\delta\delta\delta)^{TT} ttdd\Gamma + \sum(\delta\delta\delta\delta)^{TT}\, FF \quad (6)$$

The constrain constituent G can be defined in the form of penalty function:

SAMPLE

Copyright © 2025 ASME

$$G = \frac{1}{2}\int_{\Gamma_{cc}} gg^{TT}\Lambda' gg\,dd\Gamma_{cc} \tag{7}$$

where Γ_{cc} represents the contact surfaces and $\Lambda' = ddddddgg(\alpha\alpha_1, \alpha\alpha_2)$ is the penalty coefficient. gg is equation of constrain condition.

A typical situation of a contact pair is shown in the Fig. 3. Ω_1 is contactor and Ω_2 is target. The points dd and jj are hitting point and target point and FF_{ii} and FF_j are contact force. The constrain condition can be expressed in two aspects. On one hand, impenetrability is necessary for contact behavior. It means that objects Ω_1 and Ω_2 are not allowed to invade each other during the movement. Mathematically, the gap distance is non-negative:

$$gg = uu_{ii} - uu_{jj} + dd_{pp} \geq 0 \tag{8}$$

where uu_{ii}, uu_{jj} and dd_{pp} are displacements of points dd and jj and initial gap, respectively. On the other hand, the contact is separable; therefore, the normal contact force is always compressive force:

$$FF_{ii} = -FF_{jj} \geq 0 \tag{9}$$

The contact force can be calculated based on Equation (4):

$$FF_{ii} = -FF_{jj} = -\Lambda gg \tag{10}$$

combined with Equation (8):

$$FF_{ii} = -FF_{jj} = -\Lambda(uu_{ii} - uu_{jj} + dd_{pp}) \tag{11}$$

In the actual scenario, the target point is not always an element node. The displacement of target point can be calculated by the shape function and nodes displacements. Thus, the relative displacement of the contact pair is:

$$uu_{ii} - uu_{jj} = NN_{cc}dd_{cc} \tag{12}$$

where NN_{cc} and dd_{cc} are defined as:

$$NN_{cc} = [II_{2\times 2} \quad \boldsymbol{NN}] \tag{13}$$

$$dd_{cc} = [uu_{ii} \quad \boldsymbol{UU}]^{TT} \tag{14}$$

$II_{2\times 2}$ is square identity matrix with 2 by 2. $\boldsymbol{NN}$ and $\boldsymbol{UU}$ are shape function and nodes displacement of target element, respectively. In addition, the coordinate transformation matrix TT is considered when the local coordinate of contact pair does not coincide with the global one. In this manner, the contact force in global system is:

$$FF_{ii} = -FF_{jj} = -NN_{cc}^{TT}TT\Lambda TT^{TT}NN_{cc}dd_{cc} - NN_{cc}^{TT}TT\Lambda dd_{pp} \tag{15}$$

or written as:

$$FF_{ii} = -FF_{jj} = -KK_{cc}dd_{cc} + FF' \tag{16}$$

Where

$$KK_{cc} = NN_{cc}^{TT}TT\Lambda TT^{TT}NN_{cc} \tag{17}$$

$$FF' = -NN_{cc}^{TT}TT\Lambda dd_{pp} \tag{18}$$

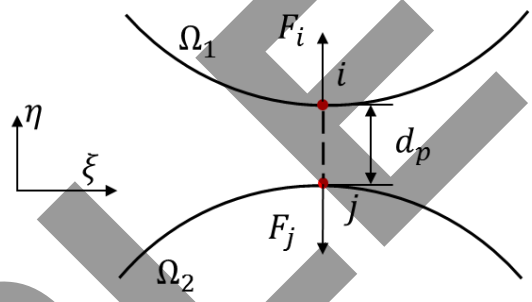

FIGURE 3: CONTACT PAIR AND THE GAP DISTANCE.

Hence, the governing equation is modified by taking account of contact as:

$$\mathbf{MM}\ddot{\boldsymbol{qq}} + \mathbf{CC}\dot{\boldsymbol{qq}} + (\mathbf{KK} + \mathbf{KK_{cc}})\boldsymbol{qq} = \mathbf{FF}(t) + \mathbf{FF}'(t) \tag{19}$$

In our proposed strategy, the central difference scheme with suitable time step is carried out to solve the second-order differential equation. The iterative equation can be expressed when zero initial conditions, i.e., $\boldsymbol{qq} = 0$ and $\dot{\boldsymbol{qq}} = 0$ at t = 0 as:

$$\frac{1}{\Delta t^2}\mathbf{MM}\boldsymbol{q}_{t+\Delta t} = [\mathbf{FF}(t) + \mathbf{FF}'(t)] - \left(\mathbf{KK} + \mathbf{KK}_{cc} - \frac{2}{\Delta t^2}\mathbf{MM}\right)\boldsymbol{q}_t - \frac{1}{\Delta t^2}\mathbf{MM}\boldsymbol{q}_{t-\Delta t} \tag{20}$$

Δt denotes the time step of integration and the damping is not considered here. The explicit algorithm is conditionally stable and the stable condition is:

$$\Delta t \leq \Delta t_{cr} = \frac{T_n}{\pi} \tag{21}$$

where Δt_{cr} is the critical stable time step and T_n denotes the minimum natural vibration period of dynamic system. It is noted that the T_n is a function of contact stiffness $\mathbf{KK_{cc}}$. Based on the definition of $\mathbf{KK_{cc}}$, the penalty coefficient $\Lambda' = ddddddgg(\alpha\alpha_1, \alpha\alpha_2)$ is a key parameter of critical stable time step. Theoretically, the accuracy of resulting solution increases as the penalty coefficient increases. However, on one hand, the great penalty coefficient brings a tough requirement on critical stable time step, which increases the computational time. On the other hand, the contact force is proportional to the coefficient. The large penalty coefficient may result in illusive reverse[13].

3. MODEL VALIDATION

SAMPLE

Copyright © 2025 ASME

To validate the developed spectral element method, a typical aluminum structure with crack is studied in this section. The dimensions of the structure and crack are illustrated in Figure 4 and the material properties are listed in Table 1. A load is induced at the left edge in the x direction by applying a boundary displacement, which is generated by a Hanning windowed sinusoidal signal with frequency 100 kHz,

$$PP(\mathrm{t}) = \frac{1}{2} PP_0 \times (1 - \cos(\frac{2\pi\pi\pi\pi}{nn} tt))\sin(2\pi\pi\pi\pi tt) \qquad (22)$$

where PP_0 is the peak value of the displacement and nn equals 5 which is the number of tunnels. The response is picked up at $xx = 0\ mm$ edge, which is the same region as the loading.

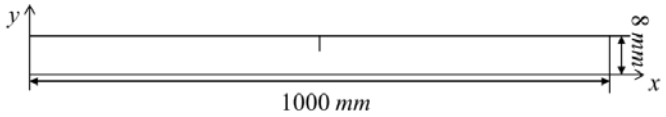

(a) THE DIMENSION OF PLATE.

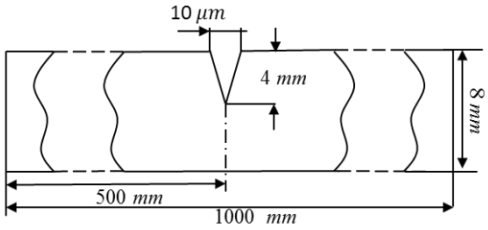

(b) THE DIMENSION OF CRACK.

FIGURE 4: THE DIMENSIONS OF A PLATE WITH CRACK.

TABLE 1: THE MATERIAL PROPERTIES OF THE STRUCTURE.

	Young's modulus E (pa)	Density (kg/mm^3)	Poisson's Ratio ν
Aluminum	7×10^{10}	2700	0.3

According to the curve of frequency thickness product, the mode of guided wave, in this case, only contains S0 and A0 modes, which can avoid the interference from other mode waves and capture the nonlinear behavior. The convergence analysis is carried out to simulate the wave propagation with a reasonable accuracy and computational cost. In this part, three mesh scales, $80 \times 4 = 320$ elements, $60 \times 4 = 240$ elements and $40 \times 4 = 160$ elements, are demonstrated in this part and the degree of interpolation is designed as 4 and the time step is chosen as $10^{-8}\ ss$. The penalty coefficient is defined as 1×10^{10} which order of magnitude is the same as it of the largest element of the stiffness matrix. As shown in Figure 5, the 240 case is the best mesh scale which can get an accurate result with a relative cost. In addition, the following results are normalized to compare the different strategies.

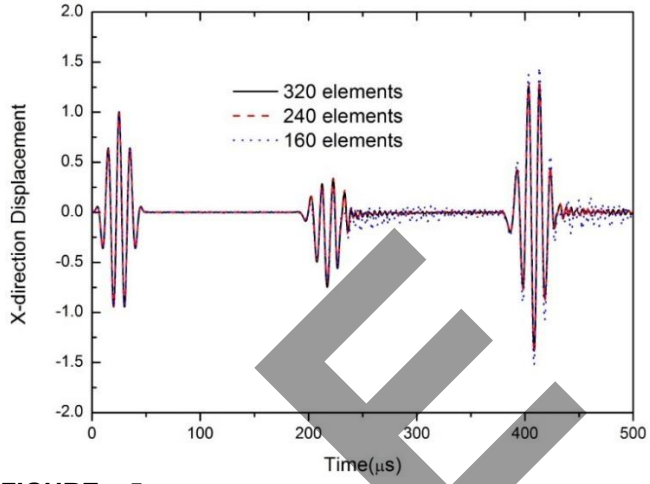

FIGURE 5: THE RESULTS OF CONVERGENCE ANALYSIS.

In addition, the commercial software ABAQUS V6.14-1 is carried out to analyze the same work scenario. Four-node bilinear quadrilateral plane strain elements are used to mesh the structure. In the case of conventional FEM, the recommendation of element size is [14]

$$l_e = \frac{\lambda_{min}}{20} \qquad (23)$$

where l_e is the element length and λ_{min} denotes the shortest interested wavelength. The breathing crack is introduced by assigning the "frictionless hard contact" function to the crack surfaces, which can simulate the crack opens and closes due to the external load. The comparison of two kinds of results is plotted in Figure 6. It is obvious that a good agreement between two results and the second wave packet is caused by the crack. The result validates the effectiveness of the developed spectral element method and contact model. In addition, the computational scales of two methods are list in Table 2. Compared with conventional FEM, the proposed approach requires less computational cast and is more effective.

TABLE 2: THE COMPUTATIONAL SCALES OF TWO METHODS.

	Number of elements	Degree of freedom	Time interval
SEM	240 (with 4th interpolation)	8210	10^{-8} s
FEM	8000	18026	10^{-8} s

SAMPLE

Copyright © 2025 ASME

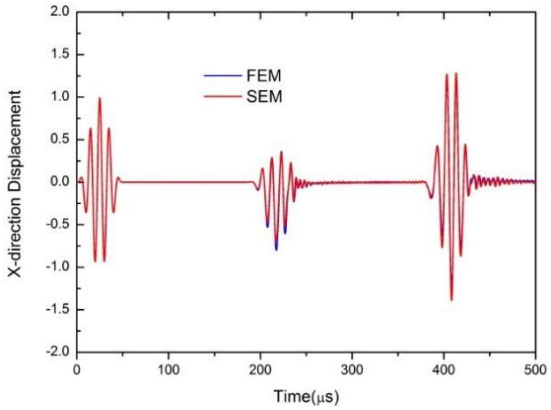

FIGURE 6: THE COMPARISON OF RESULTS OF SEM AND FEM.

4. NUMERICAL ANALYSIS OF TIME REVERSAL GUIDED WAVE

In this section, the time reversal method is carried out to detect the breathing crack of a specific model in Section 3. As shown in Fig.7, the process of time reversal consists of forward propagation and backward propagation. At first, the displacement excitation is applied at the left edge of the structure and the solution is captured at the right edge for $tt_1 = 500\mu\mu ss$. Then, this response is reversed in time domain and used as the new incident wave at the right edge for the backward propagation and the response is monitoring at the left edge, which is calculated for $2tt_1 = 1000\mu\mu ss$ to promise that the concentrated wave profile can be captured. For the sake of detecting the cracks, two structures, intact case and impaired case, are studied here.

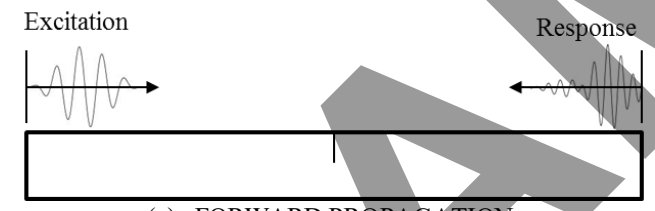

(a) FORWARD PROPAGATION



(b) BACKWARD PROPAGATION

FIGURE 7: THE PROCEDURE OF TIME REVERSAL METHOD.

The reconstructed signals obtained for the two cases are illustrated in Fig. 8. In the case of the intact structure, the profile of reconstructed signal has a good agreement with the original input signal. However, the time reversal invariance is broken in the impaired case. The envelope of time history is obviously different form other cases, which amplitude in negative is much bigger than the positive direction. The reconstructed signals of several depths of crack, 2 mm (25% depth), 4 mm (50% depth)and 6 mm (75% depth), are compared in Fig. 9. As shown in this figure, the profile of the signals is a function of relative depth of cracks and the distortion is more distinct as the crack grows, which has potential to be a damage indicator. In addition, when the excitation is applied at the right edge and the response is picked up at the left edge, the reconstructed signal is different and its maximum value is positive. This solution may result from that the breathing crack is like a 'filter', which makes the waves that open the cracks easier to pass through and those that close the cracks harder to pass. Hence, the different excitation direction results in different wave propagation although the structure is symmetric in x-axis.

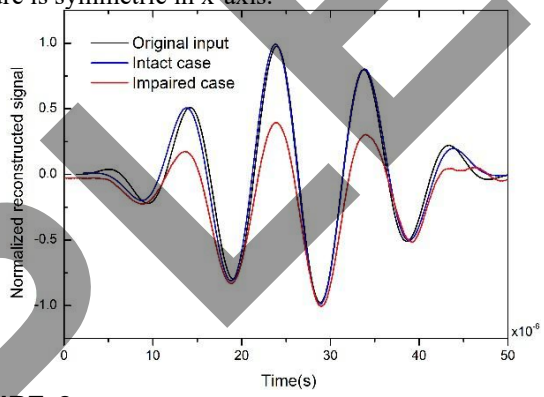

FIGURE 8: THE RECONSTRUCTED SIGNALS FOR INTACT AND IMPAIRED STRUCTURES.

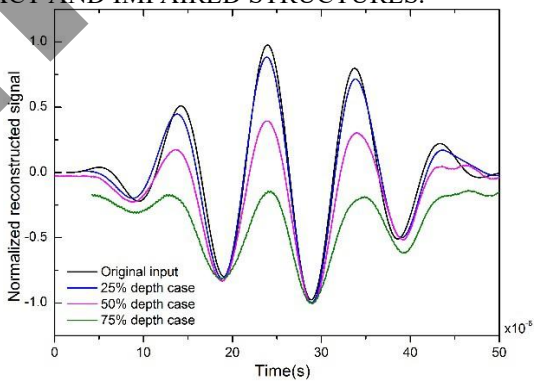

FIGURE 9: THE RECONSTRUCTED SIGNALS FOR DIFFERENT RELATIVE DEPTH.

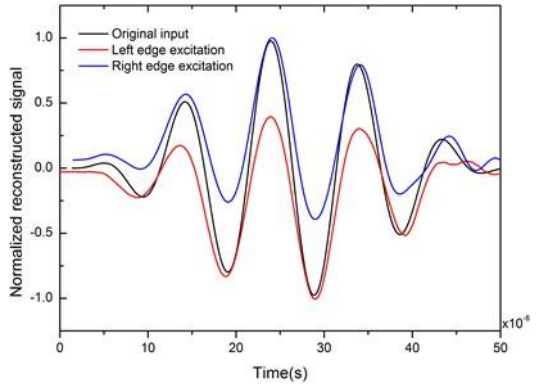

FIGURE 10: THE RECONSTRUCTED SIGNALS FOR DIFFERENT APPLIED REGION

SAMPLE

Copyright © 2025 ASME

5. CONCLUSION

In this paper, a novel strategy combined time-domain spectral element method and time reversal method is developed. By comparing the results and mesh scale of traditional FE method, the effectiveness and efficiency of the proposed method are illustrated. Based on the results of time reversal method, the reconstructed signals of intact and impaired structures are obviously different, which has the ability to be damage indicator. The results of different cases render that this strategy has the potential to reveal the depth and location of cracks.

ACKNOWLEDGEMENTS

This study is supported by the National Natural Science Foundation of China (Grant 51705422), China Postdoctoral Science Foundation (Grant 2018M633570), and Fundamental Research Funds for the Central Universities (Grant 3102017OQD004).

REFERENCES

[1] M.F. Haider, M.Y. Bhuiyan, B. Poddar, B. Lin, V. Giurgiutiu, Analytical and experimental investigation of the interaction of Lamb waves in a stiffened aluminum plate with a horizontal crack at the root of the stiffener, Journal of Sound and Vibration 431 (2018) 212-225.

[2] W. Ostachowicz, P. Kudela, M. Krawczuk, A. Zak, Guided waves in structures for SHM, J. Wiley&Sons (2012).

[3] C.H. Wang, J.T. Rose, F.K. Chang, A synthetic time-reversal imaging method for structural health monitoring, Smart Materials & Structures 13(2) (2004) 415-423.

[4] M. Fink, Time reversed acoustics, AIP Conference Proceedings, 2001.

[5] Draeger, Carsten, Theory of the time-reversal process in solids, The Journal of the Acoustical Society of America 102(3) (1997) 1289.

[6] H.W. Park, H. Sohn, K.H. Law, C.R. Farrar, Time reversal active sensing for health monitoring of a composite plate, Journal of Sound and Vibration 302(1-2) (2007) 50-66.

[7] B. Poddar, A. Kumar, M. Mitra, P.M. Mujumdar, Time reversibility of a Lamb wave for damage detection in a metallic plate, Smart Materials and Structures 20(2) (2011) 025001.

[8] F.K. Chang, Computerized time-reversal method for structural health monitoring, Nde for Health Monitoring & Diagnostics, 2003.

[9] D. Fei, B. Wu, C. He, Time reversal method for guided wave inspection in pipes, Frontiers of Mechanical Engineering in China 3(3) (2008) 251-260.

[10] A.T. Patera, A spectral element method for fluid dynamics: Laminar flow in a channel expansion, Journal of Computational Physics 54(3) (1984) 468-488.

[11] Chao Xu, Z. Yu, Numerical simulation of elastic wave propagation in functionally graded cylinders using time-domain spectral finite element method, Advances in Mechanical Engineering 9(11) (2017).

[12] W. Ostachowicz, P. Kudela, M. Krawczuk, A. Zak, Guided Waves in Structures for SHM, Wiley & Sons2011.

[13] K.J. Bathe, Finite Element Method, Wiley Encyclopedia of Conputer Science and Engineering, 2000.

[14] F. Moser, L.J. Jacobs, J. Qu, Modeling elastic wave propagation in waveguides with the finite element method, NDT&E International 32(4) (1999) 225-234.

SAMPLE

Copyright © 2025 ASME